



Article

A Risk Assessment Technique for Energy-Efficient Drones to Support Pilots and Ensure Safe Flying

Szabolcs Kocsis Szürke ¹, Norbert Perness ¹, Péter Földesi ¹, Dmytro Kurhan ², Mykola Sysyn ³
and Szabolcs Fischer ^{1,*}

¹ Central Campus Győr, Széchenyi István University, H-9026 Győr, Hungary; kocsis.szabolcs@ga.sze.hu (S.K.S.); perness.norbert.sandor@sze.hu (N.P.); foldesi@sze.hu (P.F.)

² Department of Transport Infrastructure, Ukrainian State University of Science and Technologies, UA-49005 Dnipro, Ukraine; d.m.kurhan@ust.edu.ua

³ Department of Planning and Design of Railway Infrastructure, Technical University Dresden, D-01069 Dresden, Germany; mykola.sysyn@tu-dresden.de

* Correspondence: fischersz@sze.hu; Tel.: +36-(96)-613544

Abstract: Unmanned Aerial Vehicles, also known as UAVs, play an increasingly important part in daily life. However, the ever-increasing number of UAVs pose an ever-increasing threat to the transportation infrastructure. Despite their precision and general efficiency, infrastructural-scale Unmanned Aerial Systems (UASs) have a disadvantage regarding their capability of being implanted in the ecosystem. There are several reasons for this, but the primary bottleneck is that their systems are not transparent to society and have very complicated processes. As a result, the authors decided to investigate the functional properties of UASs and make improvements to those properties. Throughout the study, the authors' primary focus was on analysis, which boosts productivity and ensures a significant level of safety for routine flights. The amount of power that a UAV uses depends on several variables, including the amount of power that its individual components require, the temperature of its surroundings, and the condition of the battery that it is powered by. Therefore, critical parameters and interdependencies are taken into account in the risk assessment strategy for energy-efficient Unmanned Aerial Vehicles (UAVs). In the case of UAVs, the algorithm performs a risk calculation before take-off to estimate the amount of risk that can be associated with the given flight time when using the provided battery. On the one hand, several instances of the pre-take-off state and how its parameters interact are investigated. On the other hand, they demonstrate the calculation of the risk while in flight, which is based on actual flight data.

Keywords: UAV; drone; risk analysis; energy-efficient flight; battery SOH; battery SOC; energy-efficient UAVs



Citation: Kocsis Szürke, S.; Perness, N.; Földesi, P.; Kurhan, D.; Sysyn, M.; Fischer, S. A Risk Assessment Technique for Energy-Efficient Drones to Support Pilots and Ensure Safe Flying. *Infrastructures* **2023**, *8*, 67. <https://doi.org/10.3390/infrastructures8040067>

Academic Editors: Ján Dižo, Rafał Melnik, Stasys Steišūnas and Miroslav Blatnický

Received: 24 February 2023

Revised: 23 March 2023

Accepted: 27 March 2023

Published: 28 March 2023



Copyright: © 2023 by the authors. Licensee MDPI, Basel, Switzerland. This article is an open access article distributed under the terms and conditions of the Creative Commons Attribution (CC BY) license (<https://creativecommons.org/licenses/by/4.0/>).

1. Introduction

Before reading this article, the authors would like to provide readers with an explanation of the potentially unusual structure of Section 1. The authors prepared Section 1 with three subsections. Section 1.1 contains a general overview of energy efficiency and emission of different areas of transport as a theoretical introduction. Section 1.2 is about Unmanned Aerial Vehicles, with a short history and the possible applications and areas, as well as an international literature review on Unmanned Aerial Vehicles in special applications. Finally, Section 1.3 was written regarding the current article's novelty, essence, and structure.

1.1. General Overview of Energy Efficiency and Emission of Different Areas of Transport

Energy efficiency is more critical in the 2020s due to the global energy crisis and rising energy prices than earlier [1]. Several articles [2–7] discuss the 2022–2023 energy crisis's

causes. Some blame the East European war, the COVID pandemic, the cyclical economy, or other socio-economic factors. However, none of these can be ruled out as the truth.

The authors start with major energy consumers to analyze energy efficiency globally and in detail. Transportation is a significant consideration [8–13]. It is important to maximize energy efficiency for all vehicles with minimal energy. From fixed-rail vehicles (trains, trams, Maglev trains, metros/underground vehicles, etc.) [14] to road vehicles, airplanes, ships, etc., the goal is to cover as much distance as possible with as little energy as possible [8,9].

Energy consumption values are usually given in kWh per passenger kilometer traveled (kWh/pkm), but Joules or Mega-Joules can also be used (J/pkm or MJ/pkm), and in freight transport, the tonnage-kilometer traveled unit is used (kWh/tkm, J/tkm, or MJ/tkm). Flight and passenger cars with petrol or diesel engines use the most energy (55–70 kWh/pkm [15]), while trams, buses, and trains use 12, 15, and 18 kWh/pkm, respectively [15]. CO₂ emissions are also significant: g/pkm and g/tkm are the units for this parameter. Airplanes and inland ships emit 285 and 245 g/pkm, while electric trains emit 14 g/tkm [14]. Trucks emit 64–693 g/tkm CO₂ (smaller trucks and vans emit more), and freight trains and inland ships emit 50 g/tkm [15]. Of course, when discussing vehicle energy efficiency and pollution, it is equally important to consider transport infrastructure construction, operation, and maintenance costs [16–23]; whole-life costs [24–26]; risk analysis of projects [27]; and infrastructure construction energy efficiency and emissions. Another possibility to reduce energy consumption is that the lower the vehicle's weight, the smaller the requested energy for driving and motion; thus, precise mechanical engineering measurement techniques can be applied. A type of this is digital image processing (DIC) [28–34], as well as shape optimization with [35] or without DIC [36].

Electric vehicles are trending now. Land [37–39], air [40–42], and water vehicles [43–45] are also necessary.

Electric vehicles are one of the greenest modes of transportation due to their low emissions. Electric vehicle research must include land, air, and water vehicles. The authors focused on drones and aircraft. They are only a portion of the aircraft industry. UAVs are booming. Drones are best for lightweight transport. The authors are creating a framework for novice and experienced pilots. This consideration is non-scientific and intended to prevent accidents and unsafe take-offs by novice pilots. Many accidents can be seen caused by risk-taking (e.g., when operating in high winds.) (Note that drones and aircraft can have other hauling/traction/driving systems besides electric ones.)

The current paper aims to investigate the risk analysis strategy for energy-efficient UAVs (the whole novelty and essence are detailed in Section 1.3). Regarding that, the authors collected the most relevant literature on this topic and prepared a short overview; it can be read in Section 1.2.

1.2. Overview of Unmanned Aerial Vehicles

1.2.1. History as Well as General and Unique Applications of Unmanned Aerial Vehicles

A drone is a widely spread term for a UAV (Unmanned Air/Aerial Vehicle), which are becoming increasingly known to everyone. First, drones were developed for warlike purposes, such as surveillance, remote bombing, and equipment dropping [46]. Then, during the 20th century, drones evolved from military to consumer electronics. In the following paragraph, the authors tried to prepare a short summary of the history of drones [47].

Austria's 1849 assault on Venice using exploding balloons may have inspired drones [47]. Austrian soldiers besieging Venice released 200 flaming balloons above the city. Each balloon carried 24–30 pounds (11.0–13.5 kg) of explosives. These balloon-dropped bombs destroyed the city below. Due to a wind shift, most balloons were blown off track; thus, just one bomb hit the Venetians. This incident was unique in military technology; however, balloons do not satisfy the modern definition of drones, particularly military drones. Nevertheless, it is fascinating to see military experts considering drones over 170 years

ago. Throughout centuries and decades, this philosophy would drive drone technology. Many commercial drones are quadcopters. In 1907, brothers Jacques and Louis Bréguet and French physiologist Professor Charles Richet invented a gyroplane, a precursor to the helicopter. The copter design was groundbreaking. The first piloted vertical-flight aircraft barely reached 0.6 m. Four men were required to stabilize the structure, making it a non-free flight [47].

Drones are employed for climate change monitoring, delivery, search and rescue, cinematography, and photography. UAVs are also becoming essential in several militaries. Twenty years later, the US military has tens of thousands of drones. Private drones dwarf this. In 2019, the FAA registered 1.1 million drones [47].

The application possibilities in the 21st century of UAVs are detailed in the following [48,49]:

- aviation;
- aerial and real estate photography, as well as videography;
- mapping and surveying, disaster zone mapping, disaster relief, and hidden area exploration;
- asset inspection and control, aerial surveillance, monitoring poachers, and insurance;
- payload carrying and parcel delivery;
- agriculture, bird control, crop spraying, crop monitoring, and precision farming;
- multispectral/thermal/NIR (near-infrared) cameras;
- live streaming events;
- roof inspections;
- emergency response, search and rescue, and marine rescue;
- forensics;
- construction and mining;
- military and firefighting;
- oil rigs and power line monitoring;
- medical applications;
- meteorology;
- wireless communication;
- and so on.

Of course, the above list does not cover all possible applications and areas. The authors did not intend to present the most exhaustive list but only to provide the reader with a sufficiently detailed overview. Special applications are discussed in Section 1.2.2.

1.2.2. International Literature Review on Unmanned Aerial Vehicles in Special Applications

Many up-to-date research fields and areas related to UAVs exist in the international literature. The most relevant ones are introduced and described shortly and concisely in the following.

Bristeau et al. [50] discuss the outcome of a project launched in 2004 by the Parrot company, the navigation and control technology embedded in the AR.Drone of commercial micro UAVs. The cost and performance of this system were outstanding in its product category, costing around EUR 300. The system uses state-of-the-art indoor navigation systems that have combined relatively inexpensive inertial sensors, computer vision, sonar, and aerodynamic models and their computation. The UAV can be remotely controlled using platforms and software running on iPhone, iPad, or iTouch devices. It has been manufactured for both civil and military use. The authors propose further improvements based on the theory of automatic control. They show that the critical points are the accuracy of vehicle position estimation and robustness. The estimation architecture established in this paper is a sophisticated combination of 70 different principles used to predict the biases and other errors of single sensors at varying timescales. The result is a complex system, but this level of complexity is not visible to the user. It emphasizes the role of automatic control as an accessible but hidden technology. Since low-level control programming algorithms have been engineered and proven to stabilize the system in sufficiently different flight

modes, it is foreseeable that control programming will play a key role in such applications through control.

Mohsan et al. [48] give a general summary of the state of UAVs globally, explaining the principles. They also mention solar and charging ensured by a laser beam. Rodríguez et al. [51] deal with UAVs in architecture, engineering, and construction (AEC), where UAVs have proven to be an optimal solution as they offer adequate performance in terms of time, precision, safety, and cost. The fields of architecture and urbanism are presented in detail. The related UASs (Unmanned Air/Aerial Systems) were described with their mapping method and recording tools. Scientific mapping was performed in two stages using sophisticated software (VOSviewerTM), with which the authors presented a scientometric and bibliometric analysis. It shows that UAVs can be valuable multi-tasking tools at any stage of an architectural project. Shariq et al. [52] developed new methods for building energy studies using advanced radiometric tools. They explored not only UAV applications. Li et al. [53] investigated a complementary optimization technique for high-atmosphere solar UAVs. It starts optimization from the drive direction and integrates the method into the general optimization technique. Weight and required power reduction are achieved by the new method. Mohan et al. [54] deal with forestation and seed spreading by UAVs; the paper discusses the topic mainly from the viewpoint of plants and soil. Aslan et al. [55] introduce an analysis and evaluation of UAS and UAS solutions in agriculture, based on other publications. González-Jorge et al. [56] provide an overview of the role of UAVs in our lives. It raises and explains agricultural, health, and monitoring opportunities. They present LiDAR (light detection and ranging) capabilities and examples. Ausonio et al. [57] discuss drone swarm methodology for forest fires. They report calculations of the critical volume of water to extinguish fires with given parameters. The paper contains calculations for the length of the suppressible fire front based on environmental factors and UAV swarm characteristics (volume, distance, and speed). Qi et al. [58] published about water–air UAVs and investigated optimal water exit angles. They discussed the flying submarine. Chamola et al. [59] introduced methods for monitoring and disabling UAS; they published no battery information review. Stek [60] issued a publication in 2014. The study focuses on the exploration by UAVs of subsurface archaeological remains in the mountainous Mediterranean landscape of Molise in southern Italy. This paper shows the preliminary data of a case study of a complex landscape site of the Classical-Roman period. Finally, the article presents a detailed study of the archaeological research and cultural heritage management potential and viability of UAVs. Specifically, it deals with the opportunities for incorporating UAV photography into current landscape archaeological research methods, such as field mapping and geophysical surveying.

The following papers deal with parcel delivery and routing, i.e., route optimization, route search, as well as UAV swarms [61–65]. Sorbelli et al. [61] investigate route planning for UAV parcel delivery, considering different winds. They address the mission feasibility problem (MFP) and investigate the effectiveness of three methodologies. These algorithms are: (i) compute the route of minimum energy once at the beginning of the mission, (ii) dynamically reconsider the most convenient trip toward the destination, and (iii) dynamically select only the best local choice. Zhang et al. [62] prepared a description and comparison of models for estimating the energy requirements of UAV parcel transport. The paper identifies the role of factors (external and UAV design) that influence energy consumption. Dorling et al. [63] investigate solving route planning challenges for parcel UAVs, improving existing route planning solutions. They published about preventing resource wastage and increasing sustainability by optimizing route and UAV design. The paper examined the optimization of battery weight based on the payload (there is sometimes more than a 10% increase in efficiency). Reyes-Rubiano et al. [64] introduced an online decision algorithm for UAV post-disaster route control. They determined three different recharge and detection tactics and their appropriate and optimal mix for the given task. The three authors considered refueling strategies to be the following: (i) extremely conservative refueling strategy (EConservative), (ii) moderately conservative refueling strategy (MConservative),

and (iii) conservative refueling strategy (Conservative). Chmaj and Selvaraj [65] discuss solutions for utilizing distributed computing environments for UAV swarms and teams. They focus on computational aspects, implementation of interoperability mechanisms between nodes of distributed systems, communication, and distributed processing principles. However, the system participants are not limited to UAVs; structures including UAV and UGV (Unmanned Ground Vehicle) participants are also included. The systems assessed in this study are not limited to the size of UAVs—systems using heavy drones, medium UAVs, mini helicopters, micro-UAVs, and others are covered. Distributed processing applications can be grouped into the following categories for the purpose of the survey: (i) general-purpose distributed processing applications, (ii) object recognition, (iii) tracking, (iv) surveillance, (v) data collection, (vi) route planning, (vii) navigation, (viii) collision avoidance, (ix) coordination, and (x) environmental monitoring. The study concludes that cooperative swarms of UAVs are more useful and have significantly better features and operational characteristics than applications running on individual UAVs. The vast majority of the cases discussed in the paper take mission-specific aspects into account. The “under the hood” level of distributed processing is left as a secondary area. They are often full of approximations and difficulties to be solved.

The following significant areas are the telecommunication systems and networks, thus, IoT (internet of things), IoE (internet of everything), mobile networks, etc. [66–70]. Liu et al. [66] deal with the description of the IoE network made available by UAVs. It details the network criteria and which UAVs can be applied. It also discusses the basics and tasks of the UAV swarm used. Yong Zeng et al. [67] demonstrate low-altitude UAV telecommunication networks. The paper describes the characteristics of obstacles and communication signals for a network in motion. Three main uses are detailed: (i) UAV-aided ubiquitous coverage, (ii) UAV-aided relaying, and (iii) UAV-aided information dissemination. Li et al. [68] show solutions for optimizing communication networks provided by UAV swarms in disaster areas. They also deal with optimizing the transmission power of all network members, as well as outages related to the movement and exchange of UAV swarms. Miao et al. [69] investigate an adaptive non-linear PI (proportional integral) controller for time linear systems. They present stability conditions and analysis of continuous faults. Improvement in settling time and continuous fault magnitude is compared to previous models. Yan et al. [70] look for the ideal battery weight of UAVs used for telecommunications purposes based on the maximum amount of energy that can be applied for telecommunications. The publication shows that horizontal and vertical flight speed and total take-off mass significantly influence the ideal battery weight.

Moreover, according to the current paper, the last but most relevant areas are the energy, energy consumption, and the energy efficiency of the UAVs [71–80]. Townsend et al. [71] compare and evaluate UAV energy sources. The advantages and disadvantages of battery, supercapacitor, solar, hydrogen, and fossil energy storage were mentioned. Hannan et al. [72] discussed the safety of UAVs; therefore, it is essential to estimate the exact charge level because in incorrectly estimated or calculated cases, the drone may not reach its target, and in the worst case, it may even crash. Chen et al. [73] present that the battery efficiency varies according to the battery’s state of charge. The efficiency is not linearly dependent on the power input. Costa et al. [74] published adequate results for Li-ion battery degradation with neural networks. There are several publications on the charging possibilities of UAVs, etc., charging with electrodes and inductive methodologies [75]; hence Chittoor et al. [76] published about an ideal inductive coil design for wireless power transmission. Another exciting approach with autonomous landing and battery on-site charging and swapping mechanisms is detailed in [77]. Fujii et al. [78] introduce the prototype development of an automated battery swap landing platform for UAVs. It uses motion-capture cameras to position and mechanically correct the UAV’s position after landing. A mechanical actuator replaces the discharged battery. Lu et al. [79] collect wireless charging technologies and test some solutions. They mention special maneuvers (e.g., gusty winds), laser charging, inductive charging, RC-coupled (RC—radio control) charging, and

battery ejector solutions. Boukoberine et al. [80] cover laser beam charging and evaluate hybrid energy storage systems. Merheb et al. [81] investigate how a UAV (more specifically, a quadcopter) with one of the four rotors completely failing during an accident in flight could be controlled by a controller. It is called a Fault Tolerant Controller (FTC). The aim is to ensure that the drone can safely continue on its planned path with the three remaining rotors. The control can be carried out with a so-called PID (Proportional–Integral–Derivative). This article demonstrates that this is indeed feasible. The loss of power, which can be detected as oscillations during flight, did not cause the drone to crash. Although the control was destroyed entirely, the presence of an activation delay, the non-symmetrical structure of the trirotor, and the odd number of rotors resulted in an unbalanced rotor torque.

Lastly, communication with drones and between drones and obtained data analysis are also significant nowadays [82–87].

1.3. Novelty, Essence, and Structure of the Current Article

The proliferation of various UAVs is a current trend, the precise regulation of which is not always well formalized. In cases where various vehicles and infrastructure elements are encountered, safe flight and risk assessment are crucial. Inaccurate weather or distance estimation might result in catastrophic accidents. Therefore, the first and most important aspect of the relationship between infrastructure and UAVs is selecting the right time and place to fly when no one is at risk. The next step is the continuous and dynamic monitoring of the flight, during which the risk value can be adjusted to the current situation. When the various drones become a permanent part of everyday life (package and food delivery, medical, and police use), communication between the infrastructure and the UAV is essential. Thus, calculating a continuous hazard index supports the decision-making of the UAV in critical situations.

The authors of this paper concentrate on analysis that improves efficiency and provides a high level of safety for regular flights. As a result, a so-called uniform scale system focusing on flight parameters was developed. A general risk factor could be defined using this scale system. Each parameter ensures that the battery is selected based on the situation, taking into account external environmental factors. To be able to validate the algorithm, simulations were run using data from real-world measurements. Based on the findings, four distinct flight categories were developed. Finally, the authors examined several examples to demonstrate the methods' applicability.

To elaborate, the method presented in this paper aims to increase the safe flight time of drones. Based on real-time data, the approach examines the expected risk and flight time before take-off, on the one hand, and the constantly changing risk, on the other. The goal is to create a tiered system for determining the risk and safety factors associated with flying drones under specific (and changing) conditions. The primary goal is to assist pilots in determining how safe it is to fly for a given mission. Another goal is to improve energy efficiency by making it simple to select the best battery for a given application once the appropriate parameters have been set. As a result, the energy required to power the battery will be neither too small nor too large.

UAVs are light in weight and require little space for battery installation. The optimal battery is a common challenge for drone builders because the more they want to fly, the more energy they require; however, more power typically requires heavier batteries, which reduces flight time.

A safety factor is a number that is assigned to the flight time. This number describes the level of safety required to carry out the actual mission. Power typically requires heavier batteries, which decreases flight time.

The structure of the paper is the following: Section 2 summarizes the materials and methods; Section 3 contains the results and discussion; finally, Section 4 is about the derived conclusions.

2. Materials and Methods

2.1. Overview of UAV Design

The quadcopter used in this article is a self-designed rotary-wing UAS. The design objective was to create a multicopter that can be operated as a digital open platform, which is well adapted to daily use in terms of dimensions, power, and take-off weight.

Its control system is the 3DR PX4 Pixhawk Advanced Autopilot running on a 32-bit ARM Cortex M4 Processor. Its accelerometer unit and redundant control supervision involving three IMUs (inertial measurement units) make it a reliable open-flight controller with sound capabilities.

It can operate in the A1/A3 open category (according to European Union standards [88]). The UAV has a dead weight of between 1700 and 2050 g, including the battery. Its MTOM (maximum take-off mass) with 12- and 14-inch propellers will result in different characteristics, so the final behavior of the UAV will be tuned to the size and inclination of the propeller. The drone will later be capable of carrying a payload of 750–1100 g.

The UAV can be used primarily for low and short-range precision flights. The multicopter can basically move and position a small gimbal and/or a microcontroller or microcomputer. The design aims to ensure that the mounted devices and their accessories can be quickly and securely mounted.

The frame is a TAROT XS 690 kit, which features a two-level layout to separate electronic components properly.

The UAS will be controlled using the 2.4 GHz ELRS (express long-range system) protocol, mainly for short- and medium-range missions. In addition, the dedicated remote control shall be configured to receive telemetry data. At the time of writing (2.5.1), the RC (radio control) module runs the latest possible secure ELRS firmware (available via ELRS Configurator). The connection between the Cube and the RX module is provided by the TELEM2 UART port using CRFS protocol.

The flight controller (FC) on a PixHawk Orange Cube FC running Ardupilot 4.3 can be updated and configured in the Mission Planner MP application.

The Mateksys integrated PDB (power distribution board) circuit is responsible for filtering the direct battery currents, branching, and routing the high-current and ESC control cables. The device uses X-Rotor, 40A 2-6S ESCs (electronic speed controllers). These are suitable for supplying power to T-Motor 3506-25, 650 KV motors (~10 A at 100% throttle). The approximate speed of the motors is 7000 rpm. The propellers are T-Motor 12 × 4 models.

The UAV is powered by 3700 mAh 4s batteries, which are LiPo (lithium-polymer) technology [89] for high-peak-current demands. The calculated flight time for one battery and the considered parameters and their values are:

- motor consumption:
 - 10.8 A per motor at 100% assumed average load;
 - 6.9 A per motor at 75% assumed average load;
 - 4.9 A per motor at 65% assumed average load;
 - 2.5 A per motor at 50% assumed average load;
- consumption of additional units:
 - 2 A assumed consumption due to control and telemetry systems;
- the expected energy demand of the construction (approximate, may vary depending on take-off weight):
 - 3.7 Ah (battery capacity)/44 A (average load)~5 min (expected flight time);
 - 3.7 Ah (battery capacity)/22 A (average load)~10 min (expected flight time);
 - 3.7 Ah (battery capacity)/11 A (average load)~20 min (expected flight time);

To be able to establish the actual consumption data, measurements were taken after the UAV was assembled, which will be described in the next section.

Figure 1 shows the completed UAV.



Figure 1. The completed UAV.

2.2. Concept of Risk Analysis and Parameter Determination

The critical parameters and interdependencies were first examined for the risk analysis. The analysis also considered the order in which they are used over time and their interaction. The block diagram in Figure 2 summarizes the main parameters and approaches used.

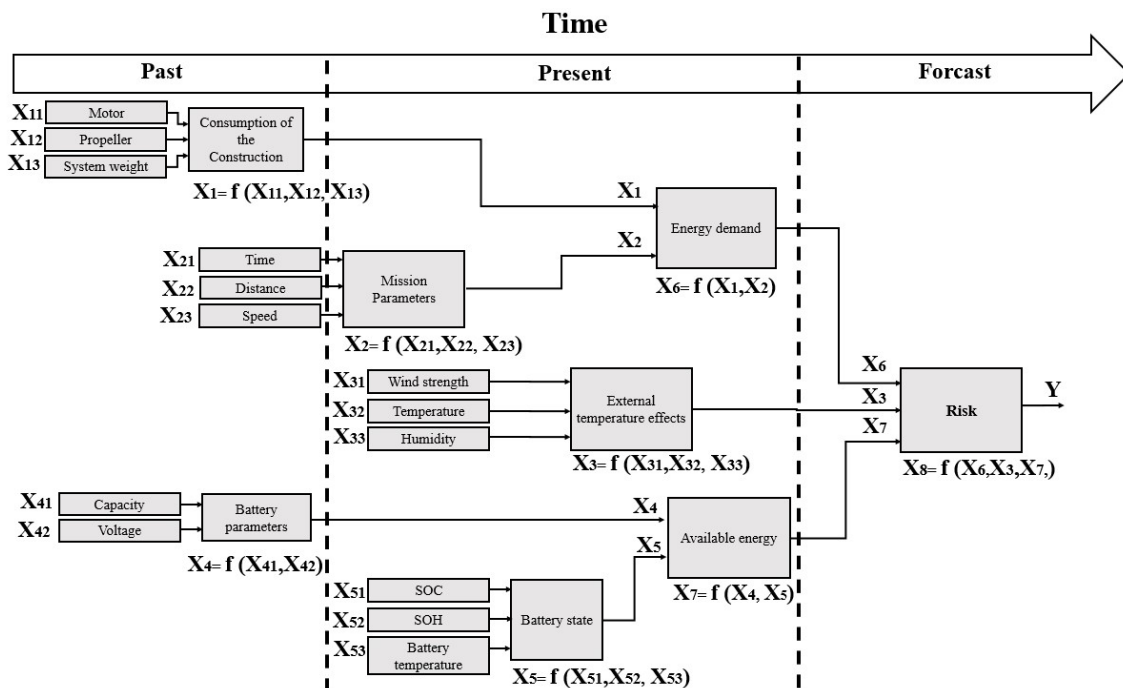


Figure 2. Risk analysis strategy for energy-efficient UAVs.

Many parameters must be considered during risk analysis. The presented case contains a lot of different parameters but shows a concise, easily understandable, and adaptable state. In the first case, the authors examine a not very complicated but sufficiently complex condition. Parameters are defined, and risks are associated using the literature [90–92] and results based on own measurements [93,94]. During the classification, the timeline was divided into past, present, and forecast (see Figure 2; in the text, these words are used in

lower cases). The parameters derived from the UAV manufacture and the battery basic data belong to the past. The present time includes current conditions and temperature components, while the forecast section determines expected conditions and safe flight times.

The input (X) parameters shown in Figure 2 depend on several things. In the previous section, the design of a UAV and its elements were presented in parts. The *Consumption of the Construction* (X_1) is influenced by several factors, the exact definition of which is a complex task. One key factor is determining the components' consumption, which can be based on catalog data as a starting point. In order to determine the consumption, it is necessary to know the *Motors* (X_{11}), the *Propellers* (X_{12}), the *System weight* (X_{13}), and possibly the controller, etc. Of course, additional items can be added (additional X_{1n} parameter), such as different sensors and cameras, but the average consumption is the critical point in all cases. For simplicity, in the first case, the catalog data were used to calculate the value of X_1 , which thus consists of the system voltage and an average load current. It is important to note that the current article does not address the design aspects and their interrelationship; it only uses the consumption context. This form of specification is part of future research. In the calculations, the average consumption was decomposed in W unit (see Equation (1)).

$$X_1 = (V_{Ns}I_{AVR}) \tag{1}$$

In Equation (1), X_1 is the system's consumption, V_{Ns} is the system's nominal voltage, and I_{AVR} is the average current. When factory data are unavailable, average consumption should be determined by measurement. Tests should be carried out under conditions that best reflect real use. It is vital to bear in mind that the replacement of individual components, e.g., engine or propeller, can have a decisive influence on consumption.

There are several options when selecting the purpose of the flight parameter (X_2). On the one hand, optimization can be carried out for *Time* in the air (X_{21}), *Distance* traveled (X_{22}), or *Speed* (X_{23}). In most cases, all three parameters are important factors, but higher speed also means higher consumption and, thus, less time in the air. The algorithm presented in this paper analyzes the time spent in the air (X_{21}); studying the distance traveled requires more minor changes in the model, while optimization for speed requires more significant changes. The approach is now to optimize for one parameter; the other values will be 0. In the case under consideration, the analysis is performed in time, so X_{22} and X_{23} are 0, and the output is determined by X_{21} (see Equation (2)).

$$X_2 = \max(X_{21}, X_{22}, X_{23}) \tag{2}$$

In Equation (2), X_2 is the expected flight time, and X_{21} is given in seconds. It is important to note that each optimization option has a different unit of measurement, so transformations will need to be made when entering values. When performing the conversion, care must be taken to ensure that the value of the X_2 parameter is second-based. Due to the different optimization conditions, in some cases the value of X_1 may vary. For example, higher average consumption may be required to achieve higher speeds. It is important to note that in the case where several parameters are to be considered, the case with the highest flight time should always be used. An essential part of future research will be further investigating different optimization options.

External temperature effects (X_3) include present and expected temperature data. It is important to note that in addition to the current components *Wind strength* (X_{31}), *Temperature* (X_{32}), and *Humidity* (X_{33}), the expected values can be found if they are available. Determining the external temperature effects for the entire flight route is vital, such as temperatures measured at different altitudes, wind speed, and relative humidity. Risk is defined as the probability of a flight failing (see Equation (3)):

$$X_3 = 1 - ((1 - X_{31})(1 - X_{32})(1 - X_{33})) \tag{3}$$

In Equation (3), X_3 is the product of *Wind strength* (X_{31}), *Temperature* (X_{32}), and *Humidity risk* (X_{33}). It is important to note that for all three external temperature parameters

X_{31} , X_{32} , and X_{33} , a risk conversion must be performed before use. The conversion for X_{31} is determined from Table 1, the conversion for X_{32} is determined from Figure 3, and the conversion for X_{33} is determined from Table 2. In all cases, the output value is between 0 and 1, as shown below. The conversion of default wind force values to risk is summarized in Table 1.

Table 1. Relation between wind force and risk values.

Speed (V_w) (km/h)	Risk Values (X_{31})
$V_w \leq 30$	0.0
$30 < V_w < 60$	0.5
$V_w \geq 60$	1.0

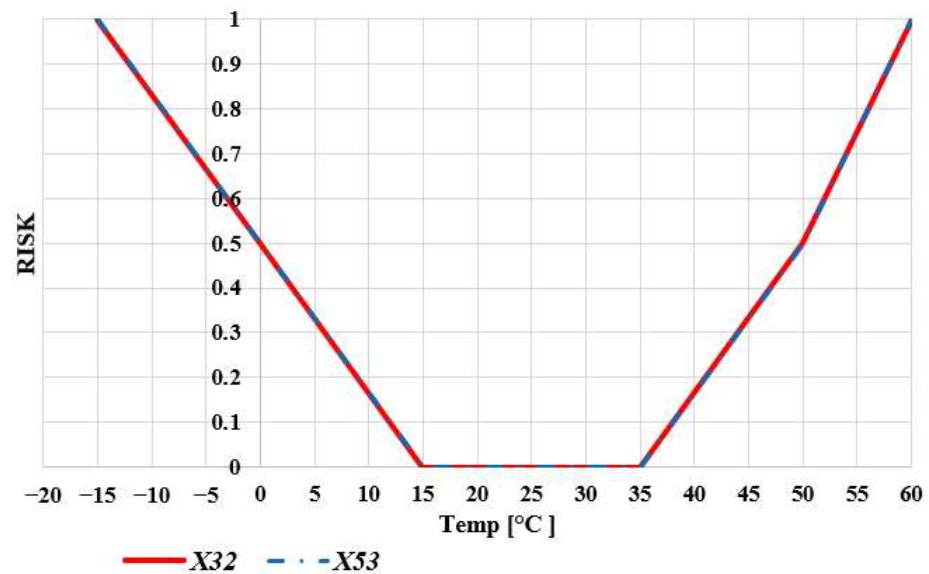


Figure 3. Relation between temperature and risk value.

Table 2. Relation between relative humidity and risk value.

Relative Humidity (RH) (%)	Risk Values (X_{33})
$RH \leq 60$	0.0
$60 < RH < 80$	0.5
$RH \geq 80$	1.0

As wind speeds (V_w) increase, it becomes more challenging to determine the exact flight time. As a function of this, higher wind strength means higher risk. Therefore, a value above 60 km/h is considered too dangerous as a starting point, regardless of wind direction. (The figures currently specified are empirical values, which may be corrected in the future after several real measurements.)

The external temperature is also an essential consideration for batteries. Too cold and too hot can both mean a drastic reduction in capacity [94]. The relationship between temperature and risk is shown in Figure 3.

Figure 3 shows that values between 15 °C and 35 °C are ideal, with cases beyond this range being increasingly risky. Take-offs below 0 °C and above 50 °C are recommended only under strong restrictions. Below -15 °C and above 60 °C, it is no longer safe to take off. The values thus defined are also based on empirical and literature recommendations and can be further refined [76,92].

Relative humidity (RH) can also significantly impact flight safety. In most cases, UAV pilots use meteorological applications to monitor the weather and reschedule flights if

possible in the case of high humidity. Table 2 shows the relationship between humidity and risk.

Based on Table 2, it can be observed that a higher relative humidity is associated with a higher risk. A relative humidity level of more than 80% is too high a risk; therefore, flying is not recommended.

After the analysis of the temperature factors and the risk conversion, X_3 can be determined, whose output is a number with no units between 0 and 1. It is important to note that the risk values are set at a default level during the approach, and pilots with more experience can adjust these values.

The concept does not consider the pilot’s driving competence and skill. As this develops, the values may naturally change. For example, a well-qualified pilot may have a different risk to a beginner. It is important to note that the approach includes baseline values; pilots with more experience can modify them. As this is a safety-oriented approach, the values are adjusted to the level of the novice UAV user.

The Battery parameters (X_4) generally contain the battery capacity and voltage values. In this case, the factory data installed on the UAV are used with the battery in its new state (see Equation (4)).

$$X_4 = (X_{41} \cdot X_{42}) \tag{4}$$

In Equation (4), X_{41} is the factory capacity in Ah of the battery and X_{42} is the nominal voltage in V. The value of X_4 is Wh.

The Battery state (X_5) values indicate the current status. The value of SOC (state of charge) (X_{51}) inbound variable, by default, specifies the assumed charge level of the current. Here, the incoming value also varies between 0 and 1, where the fully charged state means 0. Figure 4 shows the relationship between risk and charge level.

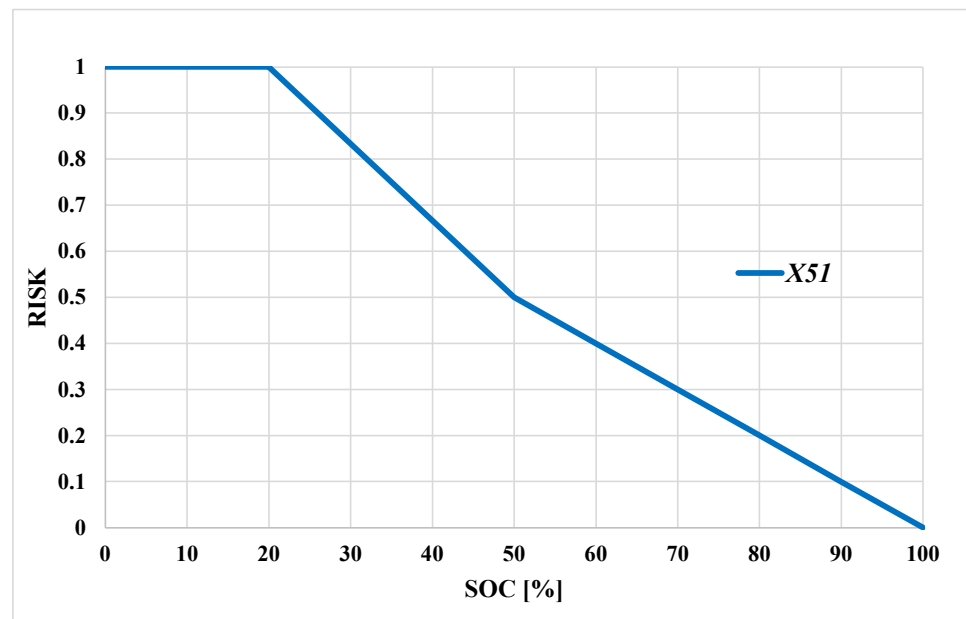


Figure 4. Relation between SOC and risk value.

In Figure 4, it can be seen that a level of occupancy below 20% is already very high risk. Due to the constantly changing conditions and the possible high peak loads, it is not recommended to land at such a low level. The lower 20% is a reserve for emergencies and should only be used after a very accurate estimation and several measurements. There is a linear increase in the correlation between SOC and risk up to 50%. With a charge level below 50%, take-off is no longer recommended, and a steeper linear section in terms of risk follows. It is important to note that in this case, the percentage of the fill level is also converted to a risk value, as shown in Figure 4, which gives the output of X_{51} .

The value of SOH (state of health) (X_{52}) is the current battery condition (see Figure 5); it is essential to note that battery wear is affected by several factors: for example, cycle number, storage, or usage. Therefore, based on the information available on the battery status, this parameter is set between 0 and 1.

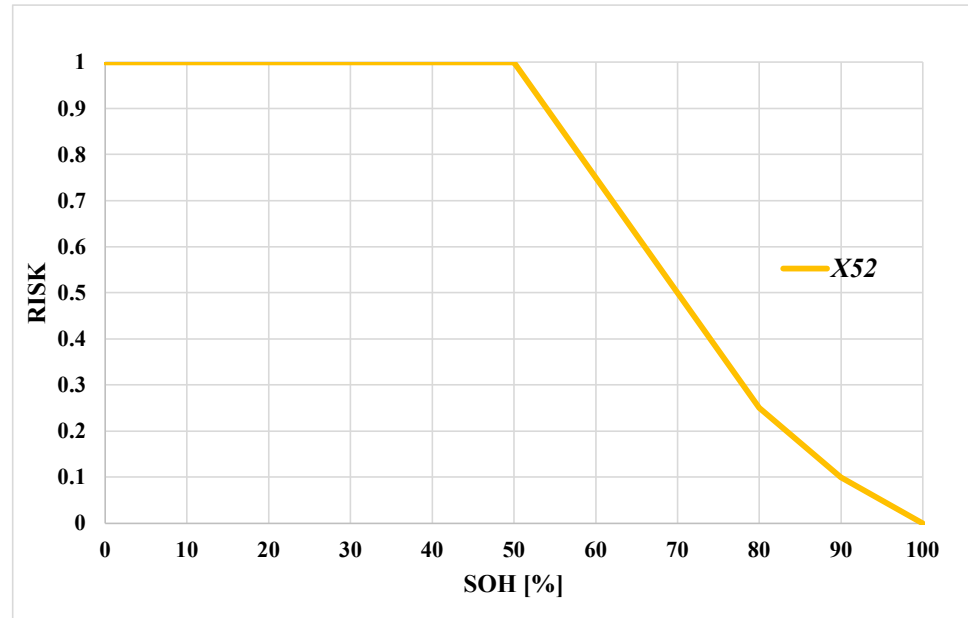


Figure 5. Relation between SOH and risk value.

In most cases, UAVs use lithium polymer batteries, the best choice for energy density, but they wear out relatively quickly. These types of batteries are no longer recommended at 50% due to the voltage drop caused by the peak load. It is important to note that at the 50% condition, when used up to 20%, only 30% of usable energy remains, according to the factory value. Therefore, a battery level of less than 70% is not recommended for safety reasons. The conversions shown in Figure 5 are based on empirical values, which can be further refined after several measurements.

The Battery temperature (X_{53}) is the present pre-take-off pack temperature. So, in this case, it indicates the current temperature of the battery and the temperature used during storage and assigns it a value of 0–1; the ideal input value is 15 °C to 35 °C. Figure 3 is a guide in terms of risk. In all cases, the first step in determining the output was to determine the risk values of the various parameters. As a function of this, the output of X_5 is (see Equation (5)):

$$X_5 = 1 - ((1 - X_{51}) \cdot (1 - X_{52}) \cdot (1 - X_{53})) \tag{5}$$

In Equation (5), the value of X_5 is the risk value between 0 and 1 calculated from the ratio of the SOC and SOH, as well as the temperature.

The Energy demand (X_6) includes the required energy to complete the current task. It is important to note that the average consumption is calculated, and peak load and its effect are not included. Furthermore, based on average consumption, the model assumes a sufficient pilot skill level to fly. Some cases are presented later in the analysis, where the effect of higher loads is analyzed in the risk calculation (see Equation (6)).

$$X_6 = (X_1 \cdot X_2) \tag{6}$$

In Equation (6), X_6 is the amount of energy in Joules that can be extracted over the expected time. The approach is based on the energy demand of the time spent in the air. So, this is the amount of energy needed to fly the UAV for the time defined by X_2 . Available

energy (X_7) is used to determine how much energy the battery has at the moment of take-off (see Equation (7)).

$$X_7 = (3600 \cdot X_4) \cdot (1 - X_5) \tag{7}$$

In Equation (7), X_7 is the currently available energy of the battery, in Joules.

The situation before take-off is analyzed first when determining the theoretical flight time. It includes energy demand, external temperature factors, and a comparison of available energy. Then, by combining the initial (factory parameters) consumption data, the current battery status, and the temperature factors, the expected flight time and the associated risk and safety factor (X_8) can be determined (see Equation (8)).

$$X_8 = 1 - \left((1 - X_3) \cdot \left(\frac{X_7}{X_6} \right) \right) \tag{8}$$

In Equation (8), X_8 is the risk of the specified flight time. If the result is 0 or below, the risk is very low, thus, 0. If it is greater than 0, further scaling is required. The value is between 0 and 1, where 1 represents the higher risk. In the evaluation, the Y-output is determined, as shown in Figure 6.

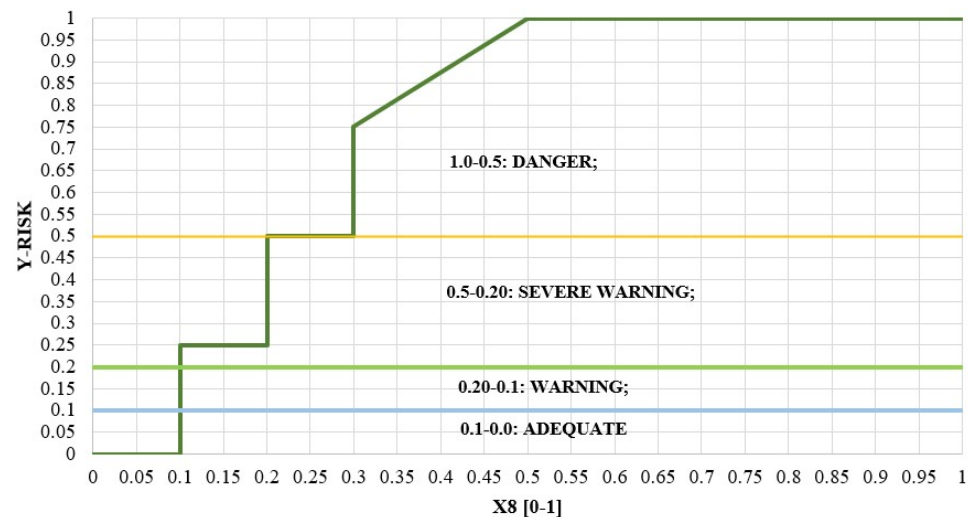


Figure 6. Determination of Y parameter.

To evaluate the value obtained after calculating X_8 , our proposed classification scheme is shown in Figure 6. It considers values between 0 and 1; where this value is less than zero, the lowest risk is assumed. It is the case, for example, if the drone can spend two–three times more time in the air than planned.

The flight can still be safely performed if the risk is not zero but not greater than 0.1. If the risk value is between 0.1 and 0.2, the take-off risk is higher, but the flight is still recommended. In case the risk is higher than 0.2, it is worth checking which parameters are not justifiable for take-off. In the case of battery condition, it is worth replacing the battery (with a new or higher capacity one), and in case of bad weather, it is worth checking whether the flight can be postponed. If the risk is greater than 0.5, delaying the flight or reducing the risk parameters is advisable.

The Y-output is a risk factor assigned to time. After determining the initial value, continuous monitoring further corrects these paired values, depending on the given situation. Since the output specifies a risk factor, the pilot can more easily make decisions about choosing flight speed. These values are objective, but it is important to note that the final decision is always in the hands of the pilot. So, it works as an aid in the background; however, it cannot interfere with flight control.

It is important to note that during the evaluation, it can be screened whether the target mission can be completed before take-off. A further advantage of this approach is that by

changing the individual parameters, for example, in the case of higher consumption, the risk factor can still be examined and calculated. Moreover, individual factors may receive a standard deviation, such as further dissection of temperature factors, as these values can change drastically quickly.

The next step is to connect the online diagnostics to the system, which allows one to compose individual values already in flight. However, it requires the continuous collection and analysis of telemetry data. Such incoming values are, e.g., the load current and cell voltage level. These values can be used to give a more accurate estimate by continuously monitoring the outside temperature. An essential complement to online diagnostics can be the use of a battery measurement database, which can further refine the assessment based on previous measurements and experience. The following section presents the continuous risk analysis of data collected from real measurements, which is the first step in online diagnostics.

3. Results and Discussion

3.1. Risk Calculation

Some examples and calculations are presented based on the risk calculation algorithm presented in the previous section. In the first case, the risk was calculated as a function of the different loads of the battery used (see Figure 7).

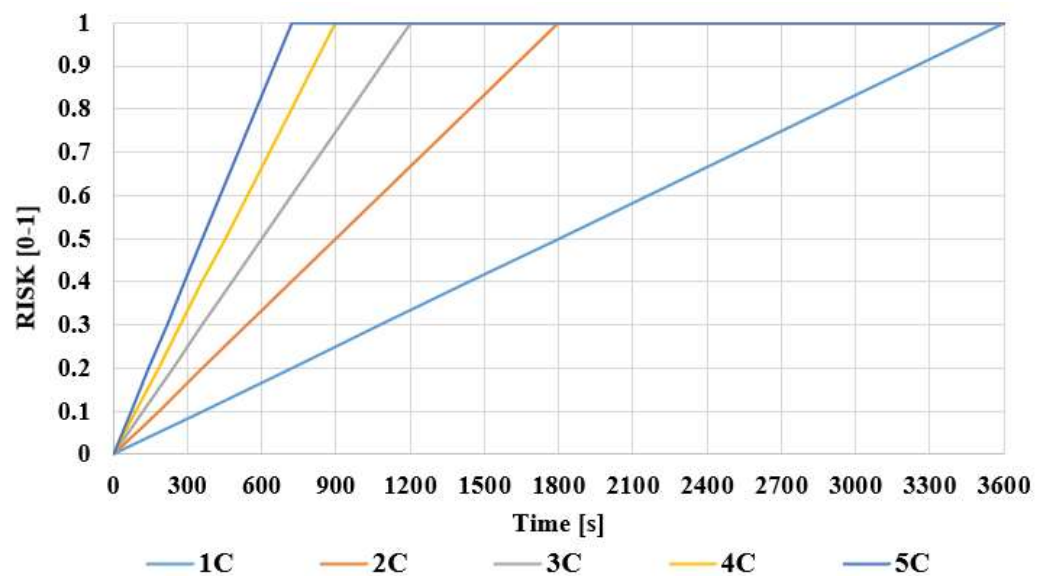


Figure 7. Analysis of the effects of different loads as a function of risk (the 1C . . . 5C values mean the discharging current; thus, if a battery is 3.7 Ah, 1C means 3.7 A discharging current, 2C means 7.4 A discharging current, and so on).

In Figure 7, it can be observed that higher loads are associated with increased risk. However, it is essential to note that the values of the discharge times are strictly theoretical, as this calculation assumes that the battery is used at 100% charge. In the following case, the different parameters were tested on each other; the analysis is based on Equation (9).

$$T_{Limit} = \frac{X_4 \cdot (1 - X_3) \cdot (1 - X_5)}{X_1} \tag{9}$$

In Equation (9), T_{Limit} is the theoretical flight time with a risk of 0, expressed in seconds. Such an evaluation can be seen in Table 3.

Table 3. Theoretical time limits (in sec unit; the meaning of 1C...5C can be seen in Figure 7).

Loading Cases	1C	2C	3C	4C	5C
Ideal	3600	1800	1200	900	720
Temp 9 °C	2880	1440	960	720	576
Temp 0 °C	1800	900	600	450	360
Temp 0 °C and wind 30 km/h	1440	720	480	360	288
SOC 90%	3240	1620	1080	810	648
SOC 80% and temp 9 °C	2304	1152	768	576	461
SOC 80%, temp 0 °C, and wind 30 km/h	720	480	192	185	144

Table 3 shows a theoretical calculation of the expected flight time based on different average impacts and factors. The first column of Table 3 shows the parameters that have been changed, e.g., in the case of temp 9 °C, only the outside temperature has been changed. On the other hand, in the case of SOC 80%, temp 0 °C, and wind 30 km/h, three parameters were modified: the battery was used up to 80%, the outside temperature was set to 0 °C, and the wind speed was 30 km/h. The next step is to perform the test based on X₂₁, which means analyzing the safety of a 1200 s flight time according to the given conditions.

Table 4 shows the pre-take-off risks at different average loads. The calculation was carried out according to Figure 1, and the output values were determined according to Figure 6. It is important to note that the presented risks indicate the pre-take-off risks and the loads at which the flight is recommended to be performed to allow the drone to spend the planned time in the air. Furthermore, 0 is the optimum value, and 1 is the most critical.

Table 4. Determination of the Y parameter regarding the C-rates (the meaning of 1C...5C can be seen in Figure 7).

Cases	1C	2C	3C	4C	5C
Ideal	0.00	0.00	0.00	0.50	0.88
Temp 9 °C	0.00	0.00	0.50	0.88	1.00
Temp 0 °C	0.00	0.50	1.00	1.00	1.00
Temp 0 °C and wind 30 km/h	0.00	0.88	1.00	1.00	1.00
SOC 90%	0.00	0.00	0.25	0.75	0.95
SOC 80% and temp 9 °C	0.00	0.00	0.81	1.00	1.00
SOC 80%, temp 0 °C, and wind 30 km/h	0.88	1.00	1.00	1.00	1.00

To be able to improve the clarity of the results, further analysis by parameters was carried out. In the three highlighted cases, the interaction of the 3C load parameters was investigated. It is important to note that for the 3C load, the system consumption is set to 11.1 A; the system voltage is 14.8 V. The planned flight time, as defined before, remained at 1200 s and was optimized for the time spent in flight. The factory values for the battery were also left unchanged at 3.7 Ah and 14.8 V. The Y-output was determined as shown in Figure 6. A more detailed parametric dependent analysis is shown in Table 5.

3.2. Measurement Results

Real measurements were taken to verify the risk calculation. The UAV used for the flight is described in detail in Section 2.1. Table 6 summarizes the values before take-off. The battery used for the flight was a new condition 3700 mAh and 14.8 V battery pack.

Table 5 summarizes the pre-take-off data, with calculations based on an estimated flight time of 1300 s. The average load was 8.2 A. Flight conditions were ideal, and the battery condition was new, but the calculation considered that 80% of the capacity was safe. Figure 8 shows the current and voltage diagram obtained from the real measurement.

Figure 8 shows the voltage in blue and the current in red. The average load was 8.2 A, corresponding to 2.2C. In Figure 9, the variation of the voltage and the SOC can be found.

Table 5. Determination of the Y parameter regarding the 3 C-rates.

Parameters	Ideal	SOC 80% and Temp 9 °C	SOC 80%, Temp 0 °C, and Wind 30 km/h
X ₁	164.28	164.28	164.28
X ₂₁	1200.00	1200.00	1200.00
X ₂	1200.00	1200.00	1200.00
X ₃₁	0.00	0.00	0.50
X ₃₂	0.00	0.20	0.50
X ₃₃	0.00	0.00	0.00
X ₃	0.00	0.20	0.75
X ₄	54.76	54.76	54.76
X ₅₁	0.00	0.00	0.00
X ₅₂	0.00	0.20	0.20
X ₅₃	0.00	0.00	0.00
X ₅	0.00	0.20	0.20
X ₆	197,136.00	197,136.00	197,136.00
X ₇	197,136.00	157,708.80	157,708.80
X ₈	0.00	0.36	0.80
Y	0.00	0.81	1.00

Table 6. Values of the parameters before take-off.

Parameters	Values
Consumption of the construction	X ₁ [W] 121.36
Mission parameters	X ₂ [s] 1300.00
External temperature effects	X ₃ [0–1] 0.00
Battery parameters	X ₄ [Wh] 54.76
Battery state	X ₅ [0–1] 0.20
Energy demand	X ₆ [J] 157,768.00
Available energy	X ₇ [J] 157,708.80
Risk	X ₈ [0–1] 0.00
Estimate flight time	T _{limit} [s] 1300.00

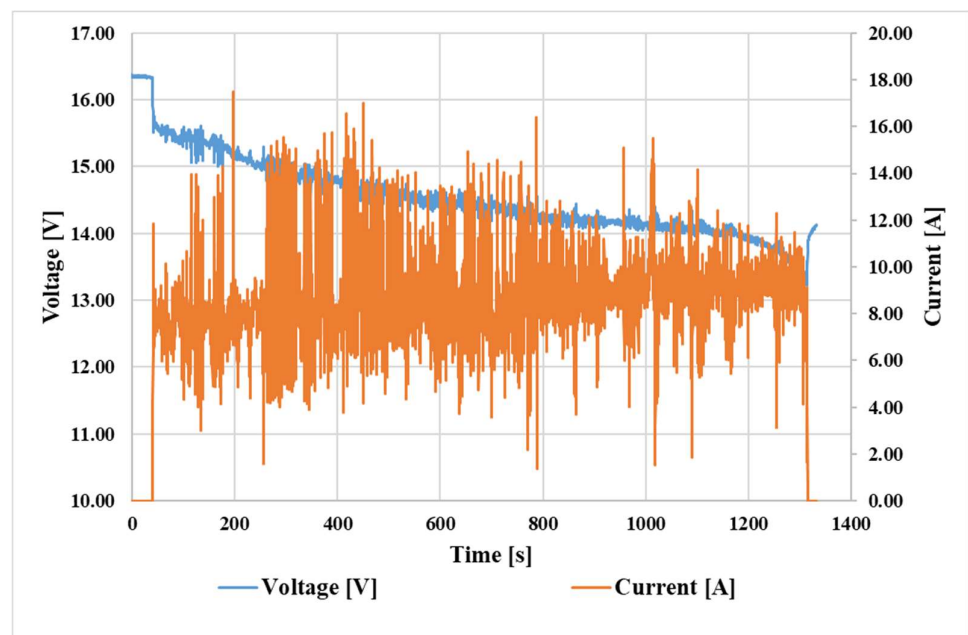


Figure 8. In-flight monitored voltage and current measurements.

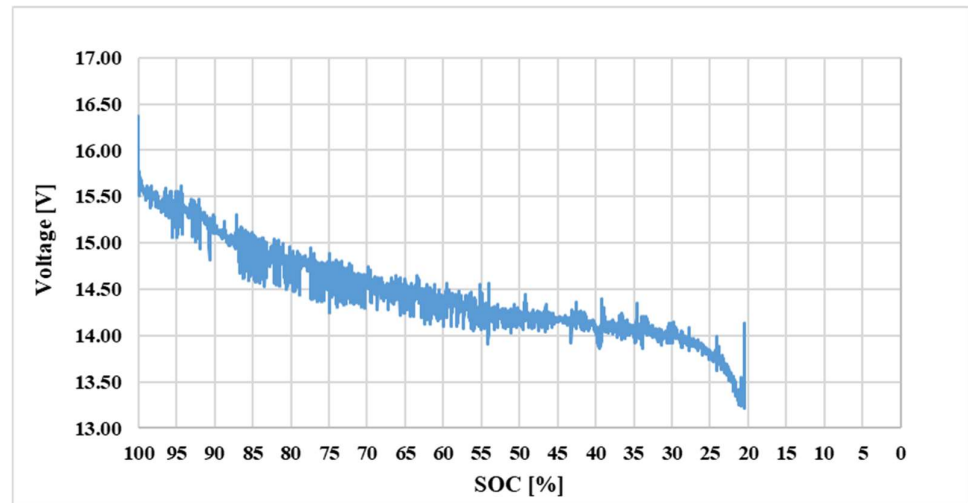


Figure 9. The voltage as a function of the SOC during the measurements.

The SOC shown in Figure 9 was determined using the Coulomb Counting method. The initial value was the nominal maximum level of the battery, and the minimum level was the limit of 20%. As a practical consideration, even in most automatic-factory setups, the last 20% SOC is not used by the UAV. Since load spikes can be dangerous below this level, usable capacity is set at 80%. Modifications had to be made to the model to determine the theoretical in-flight risk, or it depended on the battery charge and load levels. An increase in load C-rate may result, for example, from higher winds, and so on.

The relationship between risk and SOC was determined based on Figure 4, and the relationship between load magnitude and risk is shown in Figure 10.

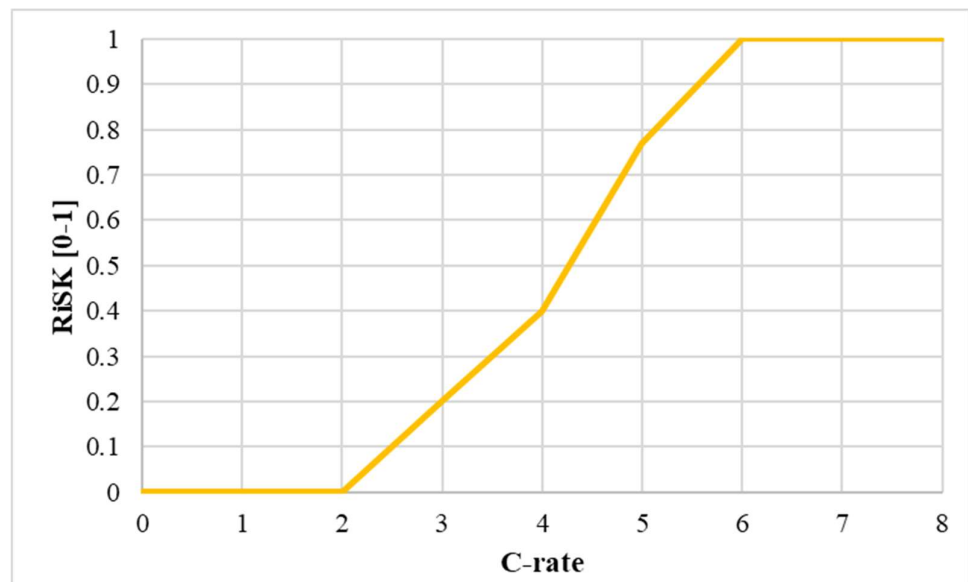


Figure 10. Relationship between risk and C-rate (the meaning of C-rate can be found in Figure 7).

The applied lithium polymer batteries can withstand very high loads, but it is essential to consider that peaks at low charge levels can be dangerous. However, as shown in Figure 10, there are no significant risks up to the 2C load.

Figure 11 shows the relationship between the voltage and risk considering the flight time based on real measurements.

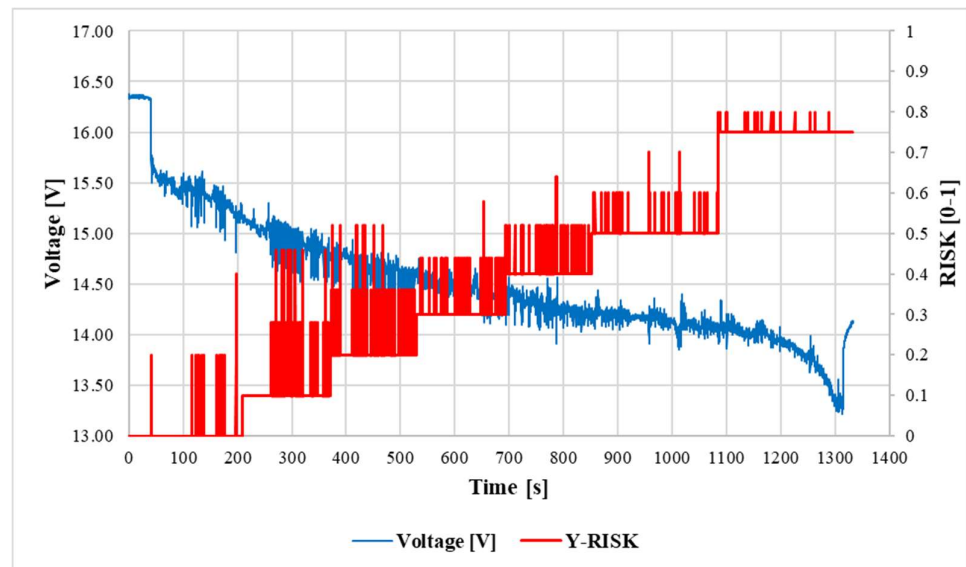


Figure 11. Relationship between the voltage and risk considering the flight time based on real measurements.

It is important to note that the risk calculated now is no longer based on the Y value defined in the previous calculations. There is a significant difference between the take-off risk and the continuously variable value defined there. Because of the continuously decreasing SOC value, the critical level, in this case, is around 20%, or 0.8 risk, where it is worth landing. The essence of the presented continuous risk estimation is to present and illustrate a simplified method for a later pilot support system.

The presented continuous risk estimator makes many simplifications that need to be modified later. Such simplifications include neglecting external factors, the voltage difference between different cells, etc.

4. Conclusions

UAVs are more commonly known and are becoming an increasingly important component of everyday life. Despite this, the increasing prevalence of UAVs poses an ever-increasing risk to the nation’s critical transportation infrastructure. Even though they have high accuracy and overall effectiveness, infrastructural-scale UASs have a disadvantage regarding their capability of being implanted in the ecosystem. The reasons for this can be explained in various ways, but the primary bottleneck is that their systems are not transparent to society and have very complicated processes. Consequently, the authors intend to research the operational properties of UAS and make improvements to those functional properties. In addition to that, they are interested in bettering the functional properties themselves. Therefore, the study’s authors placed a primary emphasis throughout the entire analysis, which not only increases productivity but also guarantees a significant level of safety for flights that are performed on a routine basis. The power consumption of a UAV is affected by several factors, such as the consumption of components, external temperature factors, and the current state of the battery used.

Significant parameters and interdependencies are taken into account within the context of the risk assessment strategy developed for energy-efficient UAVs.

In the case of UAVs, the algorithm presented in this paper calculates a risk before take-off in order to estimate how much risk the given flight time can be achieved in with the given battery. Calculation input parameters can be modified based on external factors and drone energy consumption data. In order to evaluate the proposed risk analysis algorithm, the authors created a UAV that was tested under real conditions. The risk simulation was conducted prior to the test using actual flight data.

The computational methods defined in this article can be used in flight planning, and the initial values of all parameters have been defined. It is important to note, however, that the values of each parameter can be further refined after additional real flight values. Furthermore, the values were defined assuming the pilot's qualification as beginner level.

Flight safety can be improved by simply implementing the presented elements that the pilot is aware of. In addition, using the data can prevent hazardous missions from being initiated, and during flight, the analyzing system provides the pilot with feedback to prevent further mishaps. It is essential to emphasize that the entire concept is based on individual responsibility, as the final decision regarding whether to abort a risky flight is always in the hands of the UAV operator.

An essential next step in the research will be to translate the strategy into different types of UAVs. In addition, continual in-flight status estimates and risk computations are performed. So, by expanding the concept further, dynamic risk computation may now be possible, which may considerably help a safer approach to the UAV.

Author Contributions: Conceptualization, S.K.S., N.P. and P.F.; methodology, S.K.S., N.P., P.F., D.K., M.S. and S.F.; software, S.K.S. and N.P.; validation, S.K.S., N.P., P.F., D.K., M.S. and S.F.; formal analysis, S.K.S., N.P., P.F. and S.F.; investigation, S.K.S., N.P., P.F., D.K., M.S. and S.F.; resources, S.K.S. and S.F.; data curation, S.K.S., N.P. and P.F.; writing—original draft preparation, S.K.S., N.P., P.F., D.K., M.S. and S.F.; writing—review and editing, S.K.S., N.P., P.F., D.K., M.S. and S.F.; visualization, S.K.S.; supervision, P.F., D.K., M.S. and S.F.; project administration, S.K.S. and S.F.; funding acquisition, S.K.S., P.F. and S.F. All authors have read and agreed to the published version of the manuscript.

Funding: The research carried out by Széchenyi István University was supported by the Ministry of Innovation and Technology NRD Office within the framework of the Autonomous Systems National Laboratory Program, RRF-2.3.1-21-2022-00002.

Data Availability Statement: Not applicable.

Acknowledgments: The authors thank the technical support of the related laboratories of Széchenyi István University, Győr, Hungary.

Conflicts of Interest: The authors declare no conflict of interest.

Abbreviations

AEC	architecture, engineering, and construction
DIC	digital image correlation
ECS	electronic speed controller
ELRS	express long-range system
FC	flight controller
FTC	fault tolerant controller
IMU	inertial measurement unit
IoE	internet of everything
IoT	internet of things
LiDAR	light detection and ranging
LiPo	lithium-polymer
MFP	mission feasibility problem
MTOM	maximum take-off mass
NIR	near infrared
PDB	power distribution board
PI	proportional integral
PID	proportional-integral-derivative (controller)
RC	radio control
SOC	state of charge
SOH	state of health
UAS	unmanned air/aerial systems
UAV	unmanned air/aerial vehicle
UGV	unmanned ground vehicle

Symbols	Description (meaning)	Units
X_1	consumption of the construction	W
X_{11}	UAV motor parameters in terms of consumption	W
X_{12}	UAV propeller parameters in terms of consumption	W
X_{13}	UAV system weight	kg
V_{NS}	system nominal voltage	V
I_{AVR}	average load current	A
X_2	expected flight time	S
X_{31}	wind strength risk	–
V_w	wind speed	km/h
RH	relative humidity	%
X_{32}	temperature risk	–
X_{33}	humidity risk	–
X_4	battery factory data	Wh
X_{41}	factory capacity	Ah
X_{42}	nominal voltage	V
X_5	battery state	–
X_{51}	SOC (state of charge)	%
X_{52}	SOH (state of health)	%
X_{53}	battery temperature risk	–
X_6	energy demand	J
X_7	available energy	J
X_8	risk of the specified flight time	–
Y	risk output	–
T_{LIMIT}	theoretical flight time	s

References

- Benatia, D. Ring the alarm! Electricity markets, renewables, and the pandemic. *Energy Econ.* **2022**, *106*, 105755. [CrossRef]
- Pereira, P.; Bašić, F.; Bogunovic, I.; Barcelo, D. Russian-Ukrainian war impacts the total environment. *Sci. Total Environ.* **2022**, *837*, 155865. [CrossRef] [PubMed]
- Jagtap, S.; Trollman, H.; Trollman, F.; Garcia-Garcia, G.; Parra-López, C.; Duong, L.; Martindale, W.; Munezata, P.E.S.; Lorenzo, J.M.; Hdaifeh, A.; et al. The Russia-Ukraine Conflict: Its Implications for the Global Food Supply Chains. *Foods* **2022**, *11*, 2098. [CrossRef] [PubMed]
- Kalaitezaki, A.E.; Tamiolaki, A.; Vintila, M. The Compounding Effect of COVID-19 and War in Ukraine on Mental Health: A Global Time Bomb Soon to Explode? *J. Loss Trauma* **2022**, *28*, 270–272. [CrossRef]
- Barchielli, B.; Cricenti, C.; Gallè, F.; Sabella, E.A.; Liguori, F.; Da Molin, G.; Liguori, G.; Orsi, G.B.; Giannini, A.M.; Ferracuti, S.; et al. Climate Changes, Natural Resources Depletion, COVID-19 Pandemic, and Russian-Ukrainian War: What Is the Impact on Habits Change and Mental Health? *Int. J. Environ. Res. Public Health* **2022**, *19*, 11929. [CrossRef] [PubMed]
- Basdekis, C.; Christopoulos, A.; Katsampoxakis, I.; Nastas, V. The Impact of the Ukrainian War on Stock and Energy Markets: A Wavelet Coherence Analysis. *Energies* **2022**, *15*, 8174. [CrossRef]
- Sharif, A.; Aloui, C.; Yarovaya, L. COVID-19 pandemic, oil prices, stock market, geopolitical risk and policy uncertainty nexus in the US economy: Fresh evidence from the wavelet-based approach. *Int. Rev. Financ. Anal.* **2020**, *70*, 101496. [CrossRef]
- García-Olivares, A.; Solé, J.; Osychenko, O. Transportation in a 100% renewable energy system. *Energy Convers. Manag.* **2018**, *158*, 266–285. [CrossRef]
- von Blottnitz, H.; Curran, M.A. A review of assessments conducted on bio-ethanol as a transportation fuel from a net energy, greenhouse gas, and environmental life cycle perspective. *J. Clean. Prod.* **2007**, *15*, 607–619. [CrossRef]
- Nugymanova, G.; Nurgaliyeva, M.; Zhanbirov, Z.; Naumov, V.; Taran, I. Choosing a servicing company’s strategy while interacting with freight owners at the road transport market. *Nauk. Visnyk Natsionalnoho Hirnychoho Universytetu* **2021**, 204–210. [CrossRef]
- Ramazan, B.; Mussaliyeva, R.; Bitileuova, Z.; Naumov, V.; Taran, I. Choosing the logistics chain structure for deliveries of bulk loads: Case study of the Republic Kazakhstan. *Nauk. Visnyk Natsionalnoho Hirnychoho Universytetu* **2021**, 142–147. [CrossRef]
- Tóth, C.; Primusz, P. Development of a Road Pavement Structure Diagnostic Procedure Based on the Virtual Inertial Point Method. *Coatings* **2022**, *12*, 1944. [CrossRef]
- Király, T.; Primusz, P.; Tóth, C. Simulation of Static Tyre–Pavement Interaction Using Two FE Models of Different Complexity. *Appl. Sci.* **2022**, *12*, 2388. [CrossRef]
- Fischer, S.; Kocsis Szürke, S. Detection Process of Energy Loss in Electric Railway Vehicles. *Facta Univ. Ser. Mech. Eng.* **2023**.
- KTI Ltd. Trends—Sustainable Environment. Available online: <https://www.kti.hu/trendek/fenntarthato-kornyezet/> (accessed on 21 December 2022).
- Kuchak, A.J.T.; Marinkovic, D.; Zehn, M. Parametric Investigation of a Rail Damper Design Based on a Lab-Scaled Model. *J. Vib. Eng. Technol.* **2021**, *9*, 51–60. [CrossRef]

17. Kuchak, A.T.J.; Marinkovic, D.; Zehn, M. Finite Element Model Updating—Case Study of a Rail Damper. *Struct. Eng. Mech.* **2020**, *73*, 27–35. [[CrossRef](#)]
18. Sysyn, M.; Nabochenko, O.; Kovalchuk, V.; Przybyłowicz, M.; Fischer, S. Investigation of interlocking effect of crushed stone ballast during dynamic loading. *Rep. Mech. Eng.* **2021**, *2*, 65–76. [[CrossRef](#)]
19. Szalai, S.; Eller, B.; Juhász, E.; Movahedi, M.R.; Németh, A.; Harrach, D.; Baranyai, G.; Fischer, S. Investigation of deformations of ballasted railway track during collapse using the Digital Image Correlation Method (DICM). *Rep. Mech. Eng.* **2022**, *3*, 258–282. [[CrossRef](#)]
20. Kurhan, D.; Fischer, S. Modeling of the Dynamic Rail Deflection Using Elastic Wave Propagation. *J. Appl. Comput. Mech.* **2022**, *8*, 379–387. [[CrossRef](#)]
21. Fischer, S.; Vass, A.; Szalai, S.; Harangozó, D.; Németh, A.; Major, Z.; Kocsis Szürke, S. Application Possibilities of Recuperated Energy of Modern Railway Hauling Vehicles. In Proceedings of the RAILCON'22, Nis, Serbia, 13–14 October 2022; pp. VII–X.
22. Fischer, S.; Harangozó, D.; Németh, D.; Kocsis, B.; Sysyn, M.; Kurhan, D.; Brautigam, A. Investigation of Heat-Affected Zones of Thermite Rail Weldings. *Facta Univ. Ser. Mech. Eng.* **2023**.
23. Fischer, S. Geogrid reinforcement of ballasted railway superstructure for stabilization of the railway track geometry—A case study. *Geotext. Geomembr.* **2022**, *50*, 1036–1051. [[CrossRef](#)]
24. Gáspár, L. Lifetime Engineering Principles and Durable Roads. *Int. J. Pavement Eng. Asph. Technol.* **2016**, *17*, 58–72.
25. Gáspár, L.; Bencze, Z. Long-Life Pavements—European and American Perspectives. *New Build. Mater. Constr. World* **2018**, *24*, 122–135.
26. Gáspár, L.; Horvát, F.; Lublós, L. *Közlekedési Létesítmények Élettartama*; Universitas-Győr Nonprofit Kft.: Győr, Hungary, 2011; ISBN 9789639819733.
27. Macura, D.; Laketić, M.; Pamučar, D.; Marinković, D. Risk Analysis Model with Interval Type-2 Fuzzy FMEA—Case Study of Railway Infrastructure Projects in the Republic of Serbia. *Acta Polytech. Hung.* **2022**, *19*, 103–118. [[CrossRef](#)]
28. Szalai, S.; Dogossy, G. Speckle pattern optimization for DIC technologies. *Acta Tech. Jaurinensis* **2021**, *14*, 228–243. [[CrossRef](#)]
29. Szabó, V.A.; Dogossy, G. Structure and Properties of Closed-Cell Foam Prepared from RPET. In Proceedings of the 11th Hungarian Conference on Materials Science, IOP Conference Series: Materials Science and Engineering, Balatonkenese, Hungary, 15–17 October 2017; Volume 426, p. 012043.
30. Dogossy, G.; Morauszki, T.; Ronkay, F. Experimental Investigation and Applicability of Multi-Stage Simulations in the Case of a Thick-Walled Injection-Moulded Composite. *Appl. Sci.* **2022**, *12*, 8415. [[CrossRef](#)]
31. Szalai, S.; Fehér, V.; Kurhan, D.; Németh, A.; Sysyn, M.; Fischer, S. Optimization of Surface Cleaning and Painting Methods for DIC Measurements on Automotive and Railway Aluminum Materials. *Infrastructures* **2023**, *8*, 27. [[CrossRef](#)]
32. Szalai, S.; Csótár, H.; Kurhan, D.; Németh, A.; Sysyn, M.; Fischer, S. Testing of Lubricants for DIC Tests to Measure the Forming Limit Diagrams of Aluminum Thin Sheet Materials. *Infrastructures* **2023**, *8*, 32. [[CrossRef](#)]
33. Szalai, S.; Herold, B.; Kurhan, D.; Németh, A.; Sysyn, M.; Fischer, S. Optimization of 3D Printed Rapid Prototype Deep Drawing Tools for Automotive and Railway Sheet Material Testing. *Infrastructures* **2023**, *8*, 43. [[CrossRef](#)]
34. Szalai, S.; Szívós, B.F.; Kurhan, D.; Németh, A.; Sysyn, M.; Fischer, S. Optimization of Surface Preparation and Painting Processes for Railway and Automotive Steel Sheets. *Infrastructures* **2023**, *8*, 28. [[CrossRef](#)]
35. Lamkanfi, E.; Van Paepegem, W.; Degrieck, J. Shape optimization of a cruciform geometry for biaxial testing of polymers. *Polym. Test.* **2015**, *41*, 7–16. [[CrossRef](#)]
36. Harrach, D.; Habashneh, M.; Movehdi Rad, M. Numerical Investigation of Glue Laminated Timber Beams Considering Reliability-Based Design. *Acta Polytech. Hung.* **2023**, *20*, 109–122.
37. Pup, D.; Szakallas, G.; Polák, J. Research of Vehicle Parameter and Sensor Systems Necessary to Control Autonomous Vehicles. In Proceedings of the 2018 14th IEEE/ASME International Conference on Mechatronic and Embedded Systems and Applications (MESA 2018), Oulu, Finland, 2–4 July 2018; p. 8449146.
38. Polák, J.; Lakatos, I. Efficiency Optimization of Electric Permanent Magnet Motor Driven Vehicle. *Mach. Des.* **2015**, *7*, 11–14.
39. Teichert, O.; Link, S.; Schneider, J.; Wolff, S.; Lienkamp, M. Techno-economic cell selection for battery-electric long-haul trucks. *Etransportation* **2023**, *16*, 100225. [[CrossRef](#)]
40. Ragot, P.; Markovic, M.; Perriard, Y. Optimization of Electric Motor for a Solar Airplane Application. In Proceedings of the 2005 IEEE International Conference on Electric Machines and Drives, San Antonio, TX, USA, 15–18 May 2005; IEEE: San Antonio, TX, USA; pp. 1487–1493.
41. Lefebvre, A.; Zha, G.C. Design of High Wing Loading Compact Electric Airplane Utilizing Co-Flow Jet Flow Control. In Proceedings of the 53rd AIAA Aerospace Sciences Meeting, Kissimmee, FL, USA, 5–9 January 2015; p. AIAA 2015-0772.
42. Ma, J.; Wang, S.; Wang, Y. Retrospect and Prospect of Electric Airplane in the Propulsion System, Energy Storage and Supply System. In Proceedings of the 2022 IEEE 2nd International Conference on Data Science and Computer Application (ICDSCA 2022), Dalian, China, 28–30 October 2022; IEEE: Dalian, China; pp. 819–825.
43. Khatami, R.; Chen, B.; Chen, Y.C. Optimal voyage scheduling of all-electric ships considering underwater radiated noise. *Transp. Res. Part C Emerg. Technol.* **2023**, *148*, 104024. [[CrossRef](#)]
44. Doerry, N.; Amy, J.; Krolick, C. History and the Status of Electric Ship Propulsion, Integrated Power Systems, and Future Trends in the U.S. Navy. *Proc. IEEE* **2015**, *103*, 2243–2251. [[CrossRef](#)]

45. Zahedi, B.; Norum, L.E. Modeling and Simulation of All-Electric Ships with Low-Voltage DC Hybrid Power Systems. *IEEE Trans. Power Electron.* **2012**, *28*, 4525–4537. [[CrossRef](#)]
46. The Bureau of Investigative Journalism History of Drone Warfare. Available online: <https://www.thebureauinvestigates.com/explainers/history-of-drone-warfare> (accessed on 23 December 2022).
47. Vyas, K. A Brief History of Drones: The Remote Controlled Unmanned Aerial Vehicles (UAVs). Available online: <https://interestingengineering.com/innovation/a-brief-history-of-drones-the-remote-controlled-unmanned-aerial-vehicles-uavs> (accessed on 22 March 2023).
48. Mohsan, S.A.H.; Khan, M.A.; Noor, F.; Ullah, I.; Alsharif, M.H. Towards the Unmanned Aerial Vehicles (UAVs): A Comprehensive Review. *Drones* **2022**, *6*, 147. [[CrossRef](#)]
49. RiseAbove UAV Applications and Uses. Available online: <https://riseabove.com.au/pages/uav-applications-and-uses> (accessed on 21 December 2022).
50. Bristeau, P.J.; Callou, F.; Vissière, D.; Petit, N. *The Navigation and Control Technology Inside the AR. Drone Micro UAV*; IFAC: Milano, Italy, 2011; Volume 44, ISBN 9783902661937.
51. Rodríguez, M.V.; Melgar, S.G.; Cordero, A.S.; Márquez, J.M.A. A Critical Review of Unmanned Aerial Vehicles (UAVs) Use in Architecture and Urbanism: Scientometric and Bibliometric Analysis. *Appl. Sci.* **2021**, *11*, 9966. [[CrossRef](#)]
52. Shariq, M.H.; Hughes, B.R. Revolutionising building inspection techniques to meet large-scale energy demands: A review of the state-of-the-art. *Renew. Sustain. Energy Rev.* **2020**, *130*, 109979. [[CrossRef](#)]
53. Li, X.; Sun, K.; Li, F. General optimal design of solar-powered unmanned aerial vehicle for priority considering propulsion system. *Chin. J. Aeronaut.* **2020**, *33*, 2176–2188. [[CrossRef](#)]
54. Mohan, M.; Richardson, G.; Gopan, G.; Aghai, M.M.; Bajaj, S.; Galgamuwa, G.A.P.; Vastaranta, M.; Arachchige, P.S.P.; Amorós, L.; Corte, A.P.D.; et al. UAV-Supported Forest Regeneration: Current Trends, Challenges and Implications. *Remote Sens.* **2021**, *13*, 2596. [[CrossRef](#)]
55. Aslan, M.F.; Durdu, A.; Sabanci, K.; Ropelewska, E.; Gültekin, S.S. A Comprehensive Survey of the Recent Studies with UAV for Precision Agriculture in Open Fields and Greenhouses. *Appl. Sci.* **2022**, *12*, 1047. [[CrossRef](#)]
56. González-Jorge, H.; Martínez-Sánchez, J.; Bueno, M.; Arias, P. Unmanned Aerial Systems for Civil Applications: A Review. *Drones* **2017**, *1*, 2. [[CrossRef](#)]
57. Ausonio, E.; Bagnerini, P.; Ghio, M. Drone Swarms in Fire Suppression Activities: A Conceptual Framework. *Drones* **2021**, *5*, 17. [[CrossRef](#)]
58. Qi, D.; Feng, J.F.; Liu, A.; Yang, J.; Li, Y.L. Overview on the Development and Key Technologies of Water. In Proceedings of the 2016 2nd International Conference on Control, Automation and Robotics (ICCAR), Hong Kong, China, 28–30 April 2016; pp. 213–218.
59. Chamola, V.; Kotes, P.; Agarwal, A.; Naren; Gupta, N.; Guizani, M. A Comprehensive Review of Unmanned Aerial Vehicle Attacks and Neutralization Techniques. *Ad Hoc Netw.* **2021**, *111*, 102324. [[CrossRef](#)] [[PubMed](#)]
60. Stek, T.D. Drones over Mediterranean landscapes. The potential of small UAV's (drones) for site detection and heritage management in archaeological survey projects: A case study from Le Pianelle in the Tappino Valley, Molise (Italy). *J. Cult. Herit.* **2016**, *22*, 1066–1071. [[CrossRef](#)]
61. Sorbelli, F.B.; Coro, F.; Das, S.K.; Pinotti, C.M. Energy-Constrained Delivery of Goods with Drones under Varying Wind Conditions. *IEEE Trans. Intell. Transp. Syst.* **2020**, *22*, 6048–6060. [[CrossRef](#)]
62. Zhang, J.; Campbell, J.F.; Sweeney, D.C.; Hupman, A.C. Energy consumption models for delivery drones: A comparison and assessment. *Transp. Res. Part D Transp. Environ.* **2021**, *90*, 102668. [[CrossRef](#)]
63. Dorling, K.; Heinrichs, J.; Messier, G.G.; Magierowski, S. Vehicle Routing Problems for Drone Delivery. *IEEE Trans. Syst. Man Cybern. Syst.* **2017**, *47*, 70–85. [[CrossRef](#)]
64. Reyes-Rubiano, L.; Voegl, J.; Hirsch, P. An Online Algorithm for Routing an Unmanned Aerial Vehicle for Road Network Exploration Operations after Disasters under Different Refueling Strategies. *Algorithms* **2022**, *15*, 217. [[CrossRef](#)]
65. Selvaraj, H.; Zydek, D.; Chmaj, G. Distributed Processing Applications for UAV/Drones: A Survey. In Proceedings of the Advances in Intelligent Systems and Computing, Progress in Systems Engineering: Proceedings of the Twenty-Third International Conference on Systems Engineering, ICSEng 2014, Las Vegas, NV, USA, 19–21 August 2014; Springer: Berlin, Germany; Volume 1089, pp. 449–454.
66. Liu, Y.; Dai, H.-N.; Wang, Q.; Shukla, M.K.; Imran, M. Unmanned aerial vehicle for internet of everything: Opportunities and challenges. *Comput. Commun.* **2020**, *155*, 66–83. [[CrossRef](#)]
67. Zeng, Y.; Zhang, R.; Lim, T.J. Wireless communications with unmanned aerial vehicles: Opportunities and challenges. *IEEE Commun. Mag.* **2016**, *54*, 36–42. [[CrossRef](#)]
68. Li, L.; Wen, X.; Lu, Z.; Jing, W.; Zhang, H. Energy-Efficient Multi-UAVs Deployment and Movement for Emergency Response. *IEEE Commun. Lett.* **2021**, *25*, 1625–1629. [[CrossRef](#)]
69. Miao, Q.; Wei, J.; Wang, J.; Chen, Y. Fault Diagnosis Algorithm Based on Adjustable Nonlinear PI State Observer and Its Application in UAV Fault Diagnosis. *Algorithms* **2021**, *14*, 119. [[CrossRef](#)]
70. Yan, H.; Yang, S.-H.; Chen, Y.; Fahmy, S.A. Optimum Battery Weight for Maximizing Available Energy in UAV-Enabled Wireless Communications. *IEEE Wirel. Commun. Lett.* **2021**, *10*, 1410–1413. [[CrossRef](#)]

71. Townsend, A.; Jiya, I.N.; Martinson, C.; Bessarabov, D.; Gouws, R. A comprehensive review of energy sources for unmanned aerial vehicles, their shortfalls and opportunities for improvements. *Heliyon* **2020**, *6*, e05285. [[CrossRef](#)] [[PubMed](#)]
72. Hannan, M.A.; Lipu, M.S.H.; Hussain, A.; Mohamed, A. A review of lithium-ion battery state of charge estimation and management system in electric vehicle applications: Challenges and recommendations. *Renew. Sustain. Energy Rev.* **2017**, *78*, 834–854. [[CrossRef](#)]
73. Chen, Y.; Baek, D.; Bocca, A.; Macii, A.; Macii, E.; Poncino, M. A Case for a Battery-Aware Model of Drone Energy Consumption. In Proceedings of the 2018 IEEE International Telecommunications Energy Conference (INTELEC), Torino, Italy, 7–11 October 2018; pp. 1–8.
74. Costa, E.F.; Souza, D.A.; Pinto, V.P.; Araújo, M.S.; Peixoto, A.M.; de Costa Júnior, E.P. Prediction of Lithium-Ion Battery Capacity in UAVs Erick. In Proceedings of the 2019 6th International Conference on Control, Decision and Information Technologies (CoDIT'19), Paris, France, 23–26 April 2019; pp. 1865–1869.
75. Costea, I.M.; Pleșca, V. Automatic Battery Charging System for Electric Powered Drones. In Proceedings of the 2018 IEEE 24th International Symposium for Design and Technology in Electronic Packaging (SIITME), Iași, Romania, 25–28 October 2018; pp. 377–381.
76. Chittoor, P.K.; Chokkalingam, B.; Mihet-Popa, L. A Review on UAV Wireless Charging: Fundamentals, Applications, Charging Techniques and Standards. *IEEE Access* **2021**, *9*, 69235–69266. [[CrossRef](#)]
77. Grlj, C.G.; Krznar, N.; Pranjić, M. A Decade of UAV Docking Stations: A Brief Overview of Mobile and Fixed Landing Platforms. *Drones* **2022**, *6*, 17. [[CrossRef](#)]
78. Fujii, K.; Higuchi, K.; Rekimoto, J. Endless Flyer: A Continuous Flying Drone with Automatic Battery Replacement. In Proceedings of the Proceedings—IEEE 10th International Conference on Ubiquitous Intelligence and Computing (UIC 2013) and IEEE 10th International Conference on Autonomic and Trusted Computing (ATC 2013), Sorrento Peninsula, Italy, 18–21 December 2013; pp. 216–223.
79. Lu, M.; Bagheri, M.; James, A.P.; Phung, T. Wireless Charging Techniques for UAVs: A Review, Reconceptualization, and Extension. *IEEE Access* **2018**, *6*, 29865–29884. [[CrossRef](#)]
80. Boukoberine, M.N.; Zhou, Z.; Benbouzid, M. A critical review on unmanned aerial vehicles power supply and energy management: Solutions, strategies, and prospects. *Appl. Energy* **2019**, *255*, 113823. [[CrossRef](#)]
81. Merheb, A.-R.; Noura, H.; Bateman, F. Emergency Control of AR Drone Quadrotor UAV Suffering a Total Loss of One Rotor. *IEEE/ASME Trans. Mechatron.* **2017**, *22*, 961–971. [[CrossRef](#)]
82. Tang, Q.; Yang, K.; Li, P.; Zhang, J.; Luo, Y.; Xiong, B. An energy efficient MCDS construction algorithm for wireless sensor networks. *EURASIP J. Wirel. Commun. Netw.* **2012**, *2012*, 83. [[CrossRef](#)]
83. Wang, J.; Jin, C.; Tang, Q.; Xiong, N.N.; Srivastava, G. Intelligent Ubiquitous Network Accessibility for Wireless-Powered MEC in UAV-Assisted B5G. *IEEE Trans. Netw. Sci. Eng.* **2020**, *8*, 2801–2813. [[CrossRef](#)]
84. Pu, B.; Li, K.; Li, S.; Zhu, N. Automatic Fetal Ultrasound Standard Plane Recognition Based on Deep Learning and IIoT. *IEEE Trans. Ind. Inform.* **2021**, *17*, 7771–7780. [[CrossRef](#)]
85. Wang, J.; Yang, Y.; Wang, T.; Simon Sherratt, R.; Zhang, J. Big Data Service Architecture: A Survey. *J. Internet Technol.* **2020**, *21*, 393–405.
86. Zhang, Q.; Li, Y.; Al-Turjman, F.; Zhou, X.; Yang, X. Transient ischemic attack analysis through non-contact approaches. *Hum.-Cent. Comput. Inf. Sci.* **2020**, *10*, 16. [[CrossRef](#)]
87. Zhang, J.; Zhong, S.; Wang, T.; Chao, H.C.; Wang, J. Blockchain-Based Systems and Applications: A Survey. *J. Internet Technol.* **2020**, *21*, 1–14.
88. EASA—European Union Aviation Safety Agency Open Category—Civil Drones. Available online: <https://www.easa.europa.eu/en/domains/civil-drones/drones-regulatory-framework-background/open-category-civil-drones> (accessed on 23 December 2022).
89. Szalai, S.; Szürke, S.K.; Harangozó, D.; Fischer, S. Investigation of deformations of a lithium polymer cell using the Digital Image Correlation Method (DICM). *Rep. Mech. Eng.* **2022**, *3*, 206–224. [[CrossRef](#)]
90. Alipour, M.; Ziebert, C.; Conte, F.V.; Kizilel, R. A Review on Temperature-Dependent Electrochemical Properties, Aging, and Performance of Lithium-Ion Cells. *Batteries* **2020**, *6*, 35. [[CrossRef](#)]
91. Spitthoff, L.; Shearing, P.; Burheim, O. Temperature, Ageing and Thermal Management of Lithium-Ion Batteries. *Energies* **2021**, *14*, 1248. [[CrossRef](#)]
92. Ma, S.; Jiang, M.; Tao, P.; Song, C.; Wu, J.; Wang, J.; Deng, T.; Shang, W. Temperature effect and thermal impact in lithium-ion batteries: A review. *Prog. Nat. Sci. Mater. Int.* **2018**, *28*, 653–666. [[CrossRef](#)]

93. Szürke, S.K.; Lakatos, I.; Dineva, A. Testing and Modeling Procedure of the 18650 Lithium Battery at Different Temperatures. In Proceedings of the International Symposium on Electrical Apparatus and Technologies (SIELA), Bourgas, Bulgaria, 1–4 June 2022; p. 21974594.
94. Szürke, S.K.; Szalai, S.; Lakatos, I. Battery Deformation Measurement with DIC Technique. In Proceedings of the 21st International Symposium on Electrical Apparatus & Technologies (SIELA), Bourgas, Bulgaria, 3–6 June 2020; p. 19890104.

Disclaimer/Publisher's Note: The statements, opinions and data contained in all publications are solely those of the individual author(s) and contributor(s) and not of MDPI and/or the editor(s). MDPI and/or the editor(s) disclaim responsibility for any injury to people or property resulting from any ideas, methods, instructions or products referred to in the content.